AJR FOCUS ON:

Gadoxetate Disodium–Enhanced MRI of the Liver: Part 1, Protocol Optimization and Lesion Appearance in the Noncirrhotic Liver

Kristina I. Ringe[1,2]
Daniela B. Husarik[1]
Claude B. Sirlin[3]
Elmar M. Merkle[1]

OBJECTIVE. The purpose of this article is to review the pharmacokinetic and pharmacodynamic properties of gadoxetate disodium (Gd-EOB-DTPA), to describe a workflow-optimized pulse sequence protocol, and to illustrate the imaging appearance of focal lesions in the noncirrhotic liver.

CONCLUSION. Gd-EOB-DTPA allows a comprehensive evaluation of the liver with the acquisition of both dynamic and hepatocyte phase images. This provides potential additional information, especially for the detection and characterization of small liver lesions. However, protocol optimization is necessary for improved image quality and workflow.

Keywords: gadoxetate disodium–enhanced MRI, hepatocyte-specific contrast agent, liver lesion

DOI:10.2214/AJR.10.4392

Received February 3, 2010; accepted after revision April 12, 2010.

C. B. Sirlin and E. M. Merkle are advisors to Bayer HealthCare.

[1]Department of Radiology, Duke University Medical School, Box 3808, Durham, NC 27710. Address correspondence to E. M. Merkle (elmar.merkle@duke.edu).

[2]Department of Radiology, Hannover Medical School, Hannover, Germany.

[3]Department of Radiology, University of California, San Diego, San Diego, CA.

AJR 2010; 195:13–28

0361–803X/10/1951–13

Most MRI contrast agents are based on gadolinium, a rare-earth element with strong paramagnetic properties, causing a shortening of both the T1 and T2 tissue relaxation times. On the basis of their biodistribution after IV injection, these contrast agents can be classified as purely extracellular or extracellular with a liver-specific component [1] (Table 1). Extracellular gadolinium-containing contrast agents, such as gadopentetate dimeglumine (Magnevist, Bayer HealthCare), have been in clinical use for more than two decades. Analogous to iodine-containing contrast agents used in CT, these agents are well suited for the detection and characterization of focal liver lesions because of their ability to visualize vascular perfusion [2, 3].

More recently, liver-specific contrast agents have become available for the detection and characterization of focal hepatic lesions. Currently, two contrast agents, gadoxetate disodium (Gd-EOB-DTPA, gadoxetic acid, Eovist or Primovist, Bayer HealthCare) and gadobenate dimeglumine (MultiHance, Bracco), are commercially available in the United States. These two agents are sometimes referred to as "combined contrast agents" because they have imaging properties of conventional extracellular as well as of liver-specific contrast agents [4–6]. This article will focus on the clinical applications of Gd-EOB-DTPA, reviewing the pharmacokinetic and pharmacodynamic properties of this agent, describing a workflow-optimized pulse sequence protocol, and illustrating the imaging appearance of common primary and secondary lesions in the noncirrhotic liver.

Pharmacokinetic and Pharmacodynamic Properties of Gd-EOB-DTPA

After approval in Europe and Asia as early as 2005, Gd-EOB-DTPA has been approved by the Food and Drug Administration (FDA) for use in the United States since July 2008 and is now widely available commercially. In contrast to extracellular contrast agents, Gd-EOB-DTPA shows an uptake by hepatocytes and subsequent biliary excretion. After IV injection, Gd-EOB-DTPA is transported from the extracellular space into the hepatocytes by the ATP-dependent organic anion transporting polypeptide 1 (OATP1) and subsequently excreted into the biliary canaliculi by the canalicular multispecific organic anion transporter (cMOAT). Because bilirubin is also excreted via the OATP1 receptor, the biliary excretion of Gd-EOB-DTPA depends on the overall liver function [7, 8]. In patients with normal liver and kidney function, approximately 50% of the administered dose is excreted through the hepatobiliary pathway [5, 6], with the degree of renal elimination increasing with higher doses administered [9]. The plasma half-life of Gd-EOB-DTPA is approximately 56 minutes in patients with normal hepatorenal function, which is substantially shorter compared with extracel-

lular contrast agents (e.g., gadopentetate dimeglumine plasma half-life, 96 minutes). In an animal study performed in rats, Mühler et al. [10] investigated whether Gd-EOB-DTPA can be eliminated in the absence of one of the two usual excretory pathways (urinary or biliary) and whether the remaining excretory pathway is able to compensate for impaired liver or kidney function. The authors used two groups of animals: group A underwent ligation of the common bile duct, and group B underwent ligation of the renal blood vessels. After administration of 0.1 mmol/kg of Gd-EOB-DTPA (equivalent to a quadruple dose administered in humans), most of the contrast agent was rapidly cleared from the body: 89.4% ± 7.5% of the injected dose within 4 hours after bile duct ligation via renal excretion (group A) and 87.0% ± 6.0% within 1 hour after ligation of renal vessels via biliary excretion (group B) [10].

The hepatic uptake of Gd-EOB-DTPA allows data acquisition during the hepatocyte phase in addition to the usual and earlier dynamic phase examination. Because of the marked hepatic uptake of Gd-EOB-DTPA, this hepatocyte phase is usually reached within 20 minutes after initiation of contrast injection in patients with normal hepatic function and lasts for at least 60 minutes. This long period allows the user to repeat the data acquisition during the hepatocyte phase in cases of suboptimal image quality, e.g., due to motion artifacts.

The pharmacodynamic effects of MRI contrast agents (e.g., the shortening of the T1 and T2 relaxation times) depend not only on the structure of the paramagnetic metal chelate and the degree of protein binding but also on the physiologic environment (e.g., blood, intracellular compartment, etc.) [11]. In the case of Gd-EOB-DTPA, the paramagnetic component, gadopentetate dimeglumine, is covalently linked to a lipophilic ethoxybenzyl (EOB) moiety [12]. This lipophilic moiety is not only the reason for the marked biliary excretion but also results in a relatively high protein binding of approximately 10% [13, 14].

The T1-relaxivity of Gd-EOB-DTPA is among the highest when compared with other commercially available contrast agents [11] (Table 1). The intrahepatocyte T1 relaxivity is approximately 50% higher because of reversible interactions with proteins [12]. This is of clinical importance because a substantial amount of Gd-EOB-DTPA is located within the hepatocytes when acquiring the hepatocyte phase imaging data sets.

The characteristic pharmacodynamic properties of Gd-EOB-DTPA allow a lower dosage compared with other gadolinium chelates [14]. A dosage of 0.025 mmol/kg body weight is currently approved by the FDA and recommended by the vendor. This dosage is equivalent to one quarter of the gadolinium dose recommended for all other MRI contrast agents approved by the FDA for liver imaging. This dosage is based in part on a dose-finding study performed by Vogl et al. [15] who compared Gd-EOB-DTPA given at three different doses (0.0125, 0.025, and 0.05 mmol/kg body weight) with gadopentetate dimeglumine given at a standard dose of 0.1 mmol/kg body weight in 31 patients. Compared with gadopentetate dimeglumine, similar hepatic enhancement characteristics were reported by Vogl et al. 3 minutes after injection of 0.025 and 0.05 mmol/kg body weight of Gd-EOB-DTPA, but not for the lowest dose of 0.0125 mmol/kg body weight [15]. Consequently, the FDA approved the lower, but effective, dose of 0.025 mmol/kg body weight of Gd-EOB-DTPA for use during contrast-enhanced hepatic MRI. However, the hepatic enhancement measured in that study is caused by Gd-EOB-DTPA present in the vascular and extracellular space (such as the distribution of a purely extracellular contrast agent [e.g., gadopentetate dimeglumine]) and also in the intracellular space because the hepatocyte uptake starts with the first pass and is certainly perceivable within the first 90 seconds [15]. Thus, a combination of these two effects was measured 3 minutes after injection of Gd-EOB-DTPA in the hepatic parenchyma in the dose-finding study mentioned previously, which may explain why the approved dosage of 0.025 mmol/kg body weight is currently under debate, with some radiologists preferring twice that dosage. In our practice, we often use a nondiluted dose of 10 mL of Gd-EOB-DTPA independent of the patient's weight; this approach works particularly well for fixed contrast regimens such as the triple arterial phase technique.

Protocol Optimization for Hepatobiliary Imaging With Gd-EOB-DTPA

Today, a comprehensive MR examination of the liver consists of the evaluation of the hepatic parenchyma and vasculature, detection and characterization of focal liver lesions, and assessment of the biliary ductal system. To do so, a wide range of pulse sequences is being used including single-shot T2-weighted fast spin-echo imaging, gradient-echo T1-weighted in- and opposed-phase imaging (with or without fat only and water only Dixon-based reconstructed imaging), fat-suppressed fast spin-echo T2-weighted

TABLE 1: Gadolinium-Based Contrast Agents Used for MRI of the Liver

Generic Name	Abbreviation	Drug Name	Manufacturer	Availability in United States	T1-Relaxivity in Plasma at 1.5 T ($L\ mmol^{-1}\ s^{-1}$)
Extracellular contrast agents					
Gadobutrol	Gd-BT-DO3A	Gadovist	Bayer	No	5.2
Gadodiamide	Gadopentetate dimeglumine-BMA	Omniscan	GE Healthcare	Yes	4.3
Gadopentate dimeglumine	Gadopentetate dimeglumine	Magnevist	Bayer	Yes	4.1
Gadoterate meglumine	Gadoterate meglumine	Dotarem	Guerbet	No	3.6
Gadoteridol	Gd-HP-DO3A	ProHance	Bracco	Yes	4.1
Gadoversetamide	Gadopentetate dimeglumine-BMEA	Optimark	Mallinckrodt	Yes	4.7
Hepatobiliary-specific contrast agents					
Gadobenate dimeglumine	Gadobenate dimeglumine	MultiHance	Bracco	Yes	6.3
Gadoxetate disodium	Gd-EOB-DTPA	Eovist (US)/Primovist (outside US)	Bayer	Yes	6.9

imaging, diffusion-weighted imaging (DWI), heavily T2-weighted fast spin-echo imaging to achieve an MRCP, and a dynamic series of fat-suppressed T1-weighted gradient-echo imaging before and after the administration of a gadolinium-containing contrast agent. In addition to this dynamic phase, the use of Gd-EOB-DTPA allows the acquisition of hepatocyte phase images, which can be acquired around 20 minutes after the injection of the contrast agent. A basic sequence protocol would simply add this hepatocyte phase series to the other pulse sequences. However, sequence protocol efficiency of an MR examination is important in daily clinical routine for both patient comfort and economic reasons. Thus, the time period of more than 15 minutes between the completion of the dynamic series and the acquisition of the hepatocyte phase images poses a substantial workflow problem during liver MRI with the use of Gd-EOB-DTPA. To optimize workflow, the individual pulse sequences can be reordered as given next. In addition, contrast administration regimens need to be adapted because injection volumes, relaxivity values, and the total amount of administered gadolinium molecules differ substantially with the use of Gd-EOB-DTPA [16, 17].

After the acquisition of a multiplanar localizer, all our liver MRI sequence protocols start with a 2D coronal T2-weighted single-shot fast spin-echo and a 3D T1-weighted in- and opposed-phase gradient-echo series with two-point fat only and water only Dixon reconstructions. Although we acquire T2-weighted data sets before the administration of extracellular contrast agents, we proceed straight to the dynamic series in case of Gd-EOB-DTPA.

For dynamic phase imaging, appropriate timing of the arterial phase data acquisition is of utmost importance to assess hypervascular lesions as well as to visualize the hepatic arteries and their relationship to liver masses for adequate treatment planning. Achieving excellent arterial phase imaging with Gd-EOB-DTPA is challenging because of the reduced volume of 0.1 mL/kg body weight compared with extracellular MRI contrast agents in which 0.2 mL/kg body weight is administered. In general, various strategies have been proposed to achieve adequate timing of a 3D T1-weighted gradient-echo sequence with fat suppression for the arterial phase data acquisition including a fixed delay between the initiation of the contrast administration and the start of the data acquisition, a small-volume test bolus injection to assess the circulation time between the antecubital vein and the suprarenal abdominal aorta, an automated or semiautomated bolus-detection technique, and a fixed delay combined with the acquisition of several consecutive arterial phase data sets.

Currently, the option of a fixed delay between the initiation of the contrast administration and the start of the data acquisition is not recommended because the timing of arterial enhancement is influenced by several varying factors (such as the patient's cardiac output), rendering the image quality of up to 39% of acquired arterial phase images unsatisfactory [18, 19]. The option of a small-volume test bolus also is not recommended because removal of 1–2 mL of Gd-EOB-DTPA from the prefilled syringe of 10 mL for the test bolus might not leave enough volume for administration of the recommended dose [16]. Additionally, the subsequent enhancement of the liver parenchyma resulting from the test bolus, at least theoretically, may have a negative impact on the visualization and characterization of focal liver lesions.

The main challenge in achieving good arterial phase imaging with Gd-EOB-DTPA comes from the temporal mismatch of the data acquisition (e.g., 20 seconds for a high-spatial-resolution arterial data set) and the length of the contrast bolus. If a full dose of 10 mL of Gd-EOB-DTPA is injected at 2 mL/s followed by a saline chaser (e.g., 20 mL at 2 mL/s), the bolus length initially is 5 seconds [16]. During circulation through the central veins, cardiopulmonary system, and thoracic aorta, the bolus may stretch to about 8 seconds, which is still substantially shorter than the data acquisition time. This makes adequate timing even more critical because the center of k-space filling needs to coincide with the arrival of the bolus in the main portal vein to achieve a late arterial phase. In addition, this temporal mis-

TABLE 2: Suggested 1.5-T MRI Pulse Sequence Protocol for Comprehensive Liver Examination

Pulse Sequence	Plane	TR (ms)	TE (ms)	Flip angle (°)	Field of View (mm)	Gap	Slice Thickness (mm)	Matrix
2D T2-weighted single shot FSE	Coronal	800	78	150	360	1.8	6	205 × 256
3D T1-weighted GRE (out/in phase)	Axial	7.5	2.4/4.8	10	380	0	3.5	174 × 256
3D T2-weighted FSE MRCP	Coronal	Respiratory triggered	669	140	360	0	1	384 × 381
Injection of gadoxetate disodium (0.025 mmol/kg body weight)								
3D T1-weighted GRE triple arterial phase	Axial	5.1	2.3	10	360	0	5	128 × 256
Set of three phases with no pause for breath-hold. Scanning delay depending on patient's age (< 60 y, 15 s; ≥ 60 y, 20 s)								
3D T1-weighted GRE portal venous phase	Axial	5.1	2.3	10	360	0	4	192 × 256
3D T1-weighted GRE late phase	Axial	5.1	2.3	10	360	0	4	192 × 256
Diffusion-weighted imaging	Axial	5,300	74	180	360	1.5	6	192 × 192
2D FSE T2-weighted	Axial	3,000	86	150	360	1.6	6	205 × 320
3D T1-weighted GRE hepatocyte phase	Axial	5.1	2.3	10	360	0	4	192 × 256
3D T1-weighted GRE hepatocyte phase	Coronal	5.1	2.4	30	360	0	2	179 × 256

Note—Tb values for diffusion-weighted imaging are 50 and 400 s/mm^2. Coronal 3D T1-weighted gradient-recalled echo hepatocyte phase centered over liver hilum. FSE = fast spin-echo, GRE = gradient-recalled echo.

TABLE 3: Key Points for Optimized Pulse Sequence Protocol for Hepatobiliary Imaging With Gadoxetate Disodium

Sequence	Protocol
T2-weighted MRCP	High-resolution respiratory-triggered 3D sequences should be performed before contrast injection.
	2D single-shot breath-hold sequences may be acquired immediately after portal venous phase imaging.
Arterial phase	Stretch contrast bolus by using a lower injection rate or dilute with saline.
	Alternatively, consider triple arterial phase imaging.
Fast spin-echo T2-weighted	Should be performed after contrast injection to increase contrast-to-noise ratio and to optimize workflow.
Diffusion-weighted imaging	Should be performed after contrast injection for time efficiency because there is no change in apparent diffusion coefficient values.
Hepatobiliary imaging	Acquire images 10–20 minutes after contrast injection.
	Consider an increased flip angle.
	Consider T1-weighted respiratory triggering.

match impairs the image quality (e.g., by causing truncation artifacts).

Two solutions have been proposed to address the issue of temporal mismatch. To compensate for the smaller volume, either the scanning time can be shortened or the contrast bolus can be stretched by using a lower injection rate. In an animal model, Zech et al. [20] showed that the administration of Gd-EOB-DTPA at a flow of 1 mL/s is superior to a flow of 2 mL/s with regard to arterial enhancement. Additionally, Motosugi et al. [21] showed that dilution of the contrast bolus with saline not only enlarges the injection volume and stretches the contrast bolus but also may improve the image quality because of the reduction of truncation artifacts.

Another approach to compensate for temporal mismatch is the acquisition of several consecutive arterial phases with higher temporal but lower spatial resolution. We prefer the acquisition of three consecutive arterial phases (triple-arterial) with a fixed scanning delay depending on the patient's age (15 seconds in patients younger than 60 years, 20 seconds in patients older than 60 years). Each of these arterial phase data sets is of lower spatial resolution (in-plane matrix, 128–160 × 256; slice thickness, 4–6 mm) but lasts 8 seconds only, thus matching the contrast bolus length much better (Fig. 1). The use of a triple arterial phase approach provides a late arterial phase data set (most suitable for lesion characterization) in about 95% of cases and an additional early or mid arterial data set (most suitable for vascular mapping) in an additional 65% of cases (Schulz DI et al., presented at the 2007 annual meeting of the Radiological Society of North America [RSNA]). In our experience, the availability of more than one arterial phase data set allows a more precise assessment of the arterial enhancement pattern of focal liver lesions, leading to improved characterization and diagnostic confidence.

The portal venous phase data set consists of a high-spatial-resolution 3D T1-weighted fat-suppressed gradient-echo sequence, which should be initiated as soon as the patient is ready for another breath-hold, approximately 15–20 seconds after completion of the arterial phase data acquisition. Late dynamic phase imaging is performed 2–3 minutes after contrast initiation, repeating the identical sequence used for portal venous phase imaging. Late dynamic phase imaging with Gd-EOB-DTPA is the counterpart of the equilibrium phase during MRI with extracellular agents. In the presence of Gd-EOB-DTPA, the term "equilibrium phase" is not appropriate because it applies to the use of extracellular contrast agents equally distributed among the intravascular and extravascular–extracellular compartments. Gd-EOB-DTPA, on the other hand, is distributed among four compartments within the liver, namely the intravascular space, extracellular–extravascular space, intracellular–hepatocyte space, and biliary ductal system [7]. Therefore, the term "late dynamic phase" imaging is considered more suitable for this specific data acquisition for liver-specific contrast agents, such as Gd-EOB-DTPA.

Very limited experience is currently available regarding DWI after the administration of Gd-EOB-DTPA. The University of California, San Diego, liver imaging group reported their experience in five patients in whom two different diffusion-weighted sequences were acquired before and about 2 minutes after the administration of Gd-EOB-DTPA (Rodriguez M et al., presented at the 2009 annual meeting of the International Society for Magnetic Resonance in Medicine [ISMRM]). They reported a mild increase in the apparent diffusion coefficient (ADC) after administration of Gd-EOB-DTPA for both acquisition schemes. More recently, Choi et al. [22] presented their data on DWI performed after the administration of Gd-EOB-DTPA in 34 patients with 50 focal liver lesions. Compared with unenhanced DWI, lesion-to-liver contrast was significantly higher in DWI after contrast injection, whereas there was no significant difference in mean ADC values of the focal liver lesions [22]. Thus, both studies support the approach of acquiring DWI after GD-EOB-DTPA to maintain approximately 30 minutes of overall examination time (Fig. 2).

The same holds true for T2-weighted imaging. In 80 patients with 128 liver lesions (71 hepatocellular carcinomas [HCCs], 35 metastases, and 22 hemangiomas), Kim et al. [23] performed fat-suppressed axial fast spin-echo T2-weighted imaging, both before and between 5 and 10 minutes after administration of Gd-EOB-DTPA. Although mean signal-to-noise ratios for both liver and all lesions were significantly lower on contrast-enhanced T2-weighted imaging, the contrast-to-noise ratios for liver versus solid tumors were actually significantly higher. The authors conclude that Gd-EOB-DTPA–enhanced T2-weighted images have a comparable diagnostic capability to unenhanced T2-weighted images for the detection and characterization of hepatic tumors [23]. The feasibility of T2-weighted imaging after injection of Gd-EOB-DTPA has been confirmed by several other groups (Wei JL et al., presented at the 2009 annual meeting of the

RSNA and Choi SA et al., presented at the 2009 annual meeting of the RSNA) (Fig. 3).

Excretion of Gd-EOB-DTPA into the biliary canaliculi can be seen as early as 5 minutes after contrast administration [24]. It seems reasonable to assume that a hepatocyte phase has been reached when biliary opacification is detected. Abnormal biliary contrast excretion, however, with early appearance of contrast agent in the bile ducts must be excluded as a pitfall; this can be seen in patients with vascular biliary fistulas; secondary to accidental or iatrogenic trauma; or, less often, due to vascular disorders, inflammation, or tumor [25]. Hepatocyte phase images can be acquired by applying the identical pulse sequence used for portal venous and late dynamic phase imaging. This allows excellent comparison with the other data sets acquired during the dynamic phase. Alternatively, free breathing or respiratory-triggered high-spatial-resolution T1-weighted 3D pulse sequences can be applied because acquisition speed is no longer of critical importance (Nagle SK et al., presented at the 2009 annual meeting of the ISMRM). Asbach et al. [26] recently showed that the acquisition of T1-weighted respiratory-triggered high-spatial-resolution images in the hepatocyte phase significantly improves image quality compared with breath-hold images. Hepatocyte phase imaging also benefits from a higher flip angle, which pronounces the T1 weighting of the 3D gradient-echo sequence. Usually, this flip angle ranges from 10° to 12° for dynamic liver MRI. Nagle et al. showed that a flip angle between 30° and 40° improves both hepatic and biliary imaging (Nagle SK et al., 2009 ISMRM meeting) (Fig. 4). If an MR platform does not permit adjustments of the flip angle for this specific sequence, a pulse sequence usually applied during contrast-enhanced MR angiography can be used as an alternative.

In patients with normal liver function, hepatocyte phase imaging can usually be acquired within 20 minutes after administration of Gd-EOB-DTPA [16, 27]. In patients with impaired liver function and increased bilirubin levels, however, contrast-enhanced images up to 60 minutes after injection may be necessary because Gd-EOB-DTPA competes with bilirubin at the OATP1 receptor [28].

Often, T2-weighted MRCP is part of a comprehensive MR examination of the right upper quadrant. Previous reports indicate that high concentrations of a gadolinium-containing contrast agent in the biliary ductal system may lead to signal distortion on T2-weighted images due to T2* effects of concentrated gadolinium chelates [29] (Fig. 2). We have recently shown that prior administration of Gd-EOB-DTPA adversely affects a respiratory-triggered T2-weighted 3D MRCP quantitatively and qualitatively, impairing visualization of the bile ducts [30]. The overall acquisition time of such an MRCP sequence usually is in the range of 5 minutes with the center of k-space filled at around 3 minutes (due to sequential k-space filling and partial Fourier implementation). Any biliary excretion of Gd-EOB-DTPA within the first 6–7 minutes will substantially impair the image quality of the 3D MRCP because this sequence can be implemented in the scanning protocol right after the late dynamic phase data acquisition at the earliest. Thus, the acquisition of a 3D respiratory-triggered MRCP with high spatial resolution is currently recommended before the administration of Gd-EOB-DTPA (Wei JL et al., 2009 RSNA meeting) (Fig. 5). To the best of our knowledge, breath-hold 2D single-shot MRCP sequences with acquisition times of less than 30 seconds have not been evaluated after Gd-EOB-DTPA but seem to be a reasonable alternative if acquired immediately after the portal venous phase. An exemplary MR pulse sequence protocol for comprehensive hepatobiliary imaging is provided in Table 2, and key points for imaging with Gd-EOB-DTPA are summarized in Table 3.

Detection and Characterization of Focal Liver Lesions

Because of the widespread clinical use of cross-sectional imaging, the incidence of focal liver lesions has risen over the past decade. Accurate characterization of these focal lesions combined with a high level of diagnostic confidence is necessary to select the most appropriate individual treatment strategy. The use of Gd-EOB-DTPA for liver MRI has proven to be valuable in both the detection and characterization of such lesions [31–33]. In this article, we focus on focal lesions in the noncirrhotic liver (Table 4).

Metastases

The liver is the most common site for metastases from the gastrointestinal tract, pancreas, breast, and lung [34]. Because metastatic involvement of the liver may significantly alter the therapeutic approach, exclusion of liver metastases in oncologic patients is of utmost importance. Only about 20% of metastases are solitary at the time of diagnosis. Most metastases are solid, but some may have a partial or completely cystic appearance [35]. On the basis of the degree of vascularization, differentiation between hyper- and hypovascular metastases is possible. Primary tumors with hypervascular metastases include most forms of endocrine tumors; renal cell carcinoma; and, less often, pancreatic, breast, and colon cancer [36].

At unenhanced MRI, metastases appear hypointense on T1-weighted and moderately hyperintense on T2-weighted images. After contrast injection, peripheral ring enhancement in the arterial phase with central progression, corresponding to vascular proliferation in the tumor-liver margin, can be seen in hypervascular metastases [36]. This centripetal progression of enhancement with simultaneous peripheral washout is a sign specific for malignancy [37]. In hypovascular metastases, there is no significant enhancement in the arterial phase compared with the surrounding liver parenchyma. On hepatocyte phase images, no uptake of contrast agent can be seen in hepatic metastases because these lesions do not contain hepatocytes, subsequently lacking the OATP1 transport mechanism. Gd-EOB-DTPA appears particularly suitable for the detection of very small metastases less than 1 cm in size [33, 38] and the differentiation of these very small metastases from focal nodular hyperplasia (FNH) and simple cysts (Fig. 6). Several studies have shown that Gd-EOB-DTPA–enhanced MRI depicts not only more liver metastases but also improves lesion characterization and diagnostic confidence [38–40]. However, in these studies contrast-enhanced helical CT, manganese-enhanced MRI, or superparamagnetic iron oxide particles–enhanced MRI served for comparison. To the best of our knowledge, there is currently no larger series available assessing the value of Gd-EOB-DTPA and extracellular MR contrast agents for the detection of liver metastases in a side-by-side comparison.

Hemangioma

Hemangiomas are the most common benign liver tumors and can be found in up to 20% of the general population. They are present at all ages, but are seen more frequently in premenopausal women [41], even though the association between hemangiomas and oral contraception is not fully accepted [42]. Hemangiomas are usually stable in size, ranging from 1 to 10 cm, but may grow during pregnancy and use of oral contraception

TABLE 4: Typical Imaging Appearance of Focal Liver Lesions Before and After Injection of Gadoxetate Disodium

Liver Lesion	T2-Weighted	T1-Weighted Before Injection	Arterial Phase	Hepatocyte Phase
Simple cyst	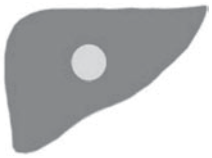	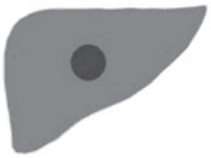	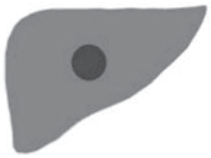	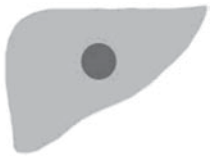
Hemangioma	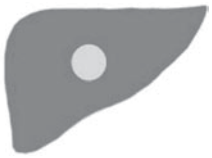	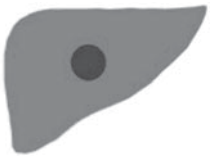	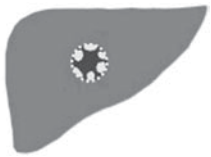	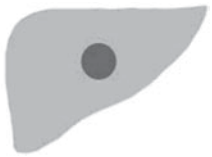
Flash-filling hemangioma	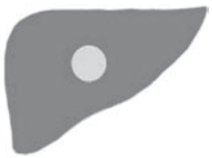	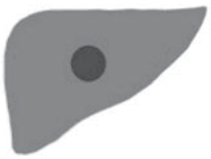	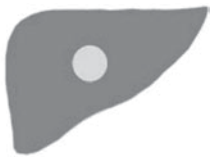	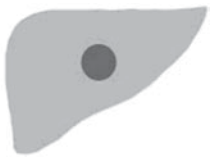
Adenoma	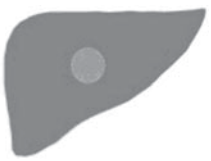		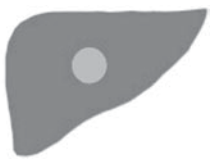	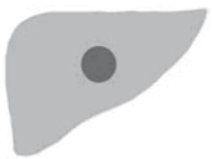
Focal nodular hyperplasia		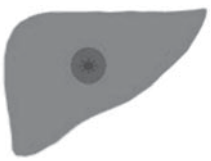	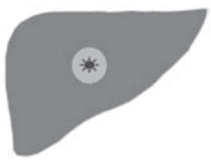	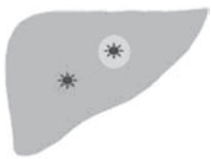
Cholangiocarcinoma	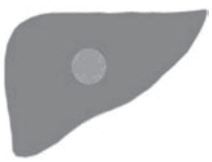		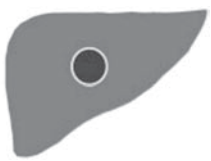	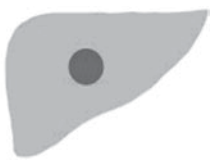
Fibrolamellar hepatocellular carcinoma	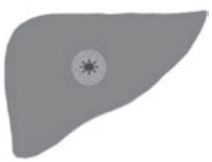		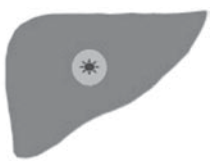	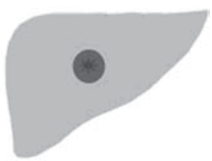
Metastasis	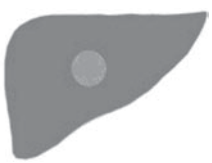	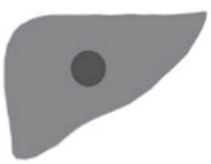	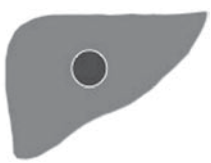	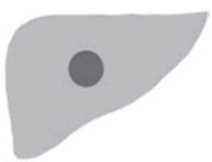

[43]. Giant hemangiomas may measure up to 20 cm. In most cases, hemangiomas are incidental findings in asymptomatic patients [44, 45].

In MRI, cavernous hemangiomas usually present as well-defined lobulated lesions, which appear hypointense on T1-weighted and profoundly hyperintense on T2-weighted images. During the dynamic phase, peripheral discontinuous nodular enhancement can be appreciated. Flash-filling capillary hemangiomas are small lesions (1–2 cm) characterized by an immediate and complete filling during the arterial phase. Although the enhancement pattern of hemangiomas during the arterial phase is similar for extracellular contrast agents and Gd-EOB-DTPA, the imaging appearance starts to differ with the portal venous phase. When extracellular agents are used, progressive centripetal filling is typical, with the lesion appearing hy-

perintense to the surrounding liver during the equilibrium and delayed phases. Usually, the signal intensity of hemangiomas aligns with the signal intensity of the portal venous branches over time because hemangiomas are composed of vascular sinusoids separated by fibrous septa [46]. With Gd-EOB-DTPA, however, hemangiomas will appear iso- or hypointense to the liver in the late dynamic phase and hepatocyte phase for three reasons: first, there is marked hepatocyte uptake of Gd-EOB-DTPA in the surrounding liver; second, the overall administered dose of Gd-EOB-DTPA is substantially lower; and third, the plasma half-life of Gd-EOB-DTPA is substantially shorter. Nevertheless, the signal intensity of a hemangioma still aligns with the signal intensity of the portal venous branches [47, 48] (Figs. 7 and 8).

Flash-filling hemangiomas may pose a serious problem because differentiation from hypervascular metastases (e.g., from neuroendocrine tumors) can be challenging because of a similar appearance in unenhanced and contrast-enhanced imaging. On the basis of limited experience, DWI may be helpful because ADC values of hemangiomas are substantially higher than ADC values of solid metastases. However, the real benefit of DWI for differentiation between small flash-filling hemangiomas and hypervascular metastases needs to be addressed in larger case series. In a given case, repeating the MR examination using an extracellular contrast agent may be necessary.

Focal Nodular Hyperplasia

FNH is the second most common benign liver tumor and is present in about 3–5% of the population. About 80% occur in women of child-bearing age [49]. FNH is considered a congenital vascular malformation, resulting in a hyperplastic response to a regenerative nonneoplastic nodule. Lesions are usually solitary (80%), with mean diameters of about 5 cm [50]. An association with the use of oral contraceptives has been described by some authors [51], whereas other studies have shown that there is no association between the use of oral contraceptives and the occurrence of FNH [52]. FNH is usually an incidental finding, only about one third of cases are diagnosed because of symptoms such as epigastric pain, abdominal mass, or hepatomegaly [50]. Histologically, an FNH shows normal hepatic parenchyma but an abnormal biliary drainage, which is not connected to the biliary ductal system of the liver. In its classical form, it is described as a nodular lesion characterized by a central stellate scar containing malformed vascular structures with radiating fibrous septa, which is macroscopically visible in about 50% of cases [53].

The radiologist's main challenge is the differentiation of FNH from hepatic adenoma and fibrolamellar carcinoma [49]. The detection on unenhanced images can be difficult, with the lesion often appearing isointense on both T1-weighted and T2-weighted images. After injection of an extracellular contrast agent or Gd-EOB-DTPA, an FNH often shows vivid enhancement resembling a spoked wheel because of its central scar and the radiating fibrous septa. On hepatocyte phase images after Gd-EOB-DTPA injection, FNH usually appears iso- or hyperintense relative to the surrounding liver parenchyma, showing the classic popcornlike enhancement pattern because of the accumulation of Gd-EOB-DTPA and poor biliary drainage [54, 55]. The central scar, however, appears different when using an extracellular agent or Gd-EOB-DTPA. Because the central stellate scar contains malformed vascular structures, it shows enhancement characteristics similar to hemangiomas, appearing hyperintense on delayed phase imaging using extracellular agents but hypointense on hepatocyte phase images using Gd-EOB-DTPA (Fig. 9).

Hepatic Adenoma

Hepatic adenomas are rare liver lesions occurring especially in women taking oral contraceptives [56], with a female-to-male ratio of 5:1 [57]. Multiple adenomas can be associated with diabetes mellitus, glycogen storage disease type 1 and 3, and consumption of anabolic or androgenic steroids [58, 59], whereas liver adenomatosis is defined as the presence of more than 10 adenomas in an otherwise normal liver in patients with no history of steroid intake or metabolic disease [60]. Adenomas vary in size from 1 to 10 cm and can regress after cessation of oral contraceptive use. Although most patients are asymptomatic, larger adenomas may cause abdominal discomfort. Hemorrhage constitutes the main complication of adenomas, and spontaneous rupture and hemoperitoneum occur in up to 10% of cases, especially during menstruation, pregnancy, or postpartum [61]. Malignant transformation to HCC is estimated to occur in about 5% [62, 63]. Because of the risks of rupture and possible malignant transformation, differentiation from lesions such as FNH or hemangioma is paramount [64].

Pathologically, hepatic adenomas are characterized by benign proliferation of hepatocytes separated by dilated sinusoids and enclosed by a pseudocapsule. Intratumoral fat, necrosis, hemorrhage, or large subcapsular vessels are commonly observed [65]. Hepatic adenomas do not contain bile ducts (a key histologic finding distinguishing them from FNH), resulting in blocked bilirubin excretion [66].

Because of hemorrhage or intralesional fat, adenomas frequently appear heterogeneously hyperintense on unenhanced T1-weighted images. On opposed-phase images, signal loss because of fatty components may be appreciated. After injection of Gd-EOB-DTPA, hepatic adenomas frequently enhance in the arterial phase, with a washout in later phases. On hepatocyte phase images, adenomas typically appear hypointense because of the lack of biliary canaliculi, a main feature differentiating hepatic adenomas from FNH, as has been shown by several studies using gadobenate dimeglumine [67]. However, adenomas can occasionally appear iso- or even hyperintense to the liver on hepatocyte phase imaging, with the underlying transport mechanism poorly understood (Fig. 10). To the best of our knowledge, no larger series are currently available looking specifically at MRI of hepatic adenomas with Gd-EOB-DTPA.

Cholangiocarcinoma

Cholangiocarcinoma is the second most common form of primary hepatic malignancy. It derives from the biliary epithelium, arising as adenocarcinoma, papillary carcinoma, or mucinous carcinoma [68]. Depending on its side of origin, it is either classified as intra- or extrahepatic cholangiocarcinoma, with the intrahepatic tumors further divided into peripheral or central (Klatskin) cholangiocarcinoma [69]. Two thirds of cholangiocarcinomas involve the extrahepatic bile ducts. Risk factors for the development of cholangiocarcinoma include primary sclerosing cholangitis (PSC), familial polyposis, choledochal cyst, biliary papillomatosis, and clonorchiasis [70]. In a PSC patient, the risk for developing cholangiocarcinoma is approximately 1.5% per year after diagnosis of cholestatic liver disease [71]. Most patients with cholangiocarcinoma present with obstructive jaundice. Additional symptoms occur in about one third of cases and may include pruritus, abdominal pain, weight loss, and fever. Liver function tests and tumor markers may be elevated [72].

On the basis of morphologic characteristics, intrahepatic cholangiocarcinoma can be classified into mass-forming, periductal infiltrating, and intraductal growing types [73, 74]. At MRI, mass-forming cholangiocarcinoma appears hypointense on T1-weighted and mild to moderately hyperintense on T2-weighted images, depending on the amount of fibrous tissue and mucin content. Irregular peripheral rim enhancement during the arterial phase may be appreciated after injection of Gd-EOB-DTPA. Because of its fibrous components, delayed washout is typical for cholangiocarcinoma when extracellular contrast agents are used. In the presence of Gd-EOB-DTPA, however, the surrounding liver enhances more because of the hepatocyte uptake, thus causing the cholangiocarcinoma to appear hypointense to the background liver. Preliminary experience suggests that this hypointense appearance of cholangiocarcinoma allows better lesion demarcation, which can be rather difficult in the presence of extracellular agents.

Associated findings may include capsular retraction, satellite nodule, vascular encasement, and hepatolithiasis. Diffuse periductal thickening with increased enhancement and abnormally dilated or irregularly narrowed ducts can be seen in periductal infiltrating types, whereas duct dilation associated with an intraductal mass that enhances after contrast injection may be seen in case of intraductal cholangiocarcinoma [74]. Decreased uptake of Gd-EOB-DTPA in the parenchyma surrounding the tumor is indicative of decreased hepatocyte function (Fig. 11).

Fibrolamellar HCC

Fibrolamellar HCC is a distinctive subtype of primary HCC, generally occurring in young patients (average age, 25 years) without chronic liver disease or other risk factors for HCC. It accounts for about 1–2% of all HCC cases in the United States [75]. The exact cause is unknown. Fibrolamellar HCCs are usually solitary lesions and are detected when they are large (5–20 cm). The clinical presentation is generally nonspecific, with patients presenting with symptoms such as nausea, abdominal discomfort, weight loss, or jaundice. Histologically, fibrolamellar HCC is composed of well-differentiated, enlarged neoplastic hepatocytes surrounded by abundant thick fibrous bands, which are often arranged in parallel or lamellar distribution [75].

The MRI appearance of fibrolamellar HCC is heterogeneous, with the tumor being hypo- or isointense on T1-weighted images and moderately hyperintense on T2-weighted images. A central stellate scar may be seen in up to 60% of cases. This scar is predominantly hypointense on T1-weighted images, with heterogeneous enhancement in the arterial phase. Calcification of the scar can be appreciated in up to 50% of cases [76]. Compared with FNH, the central scar is generally larger, more irregular, and more heterogeneous in signal intensity and contrast enhancement [77]. On hepatocyte phase images, fibrolamellar HCC appears predominantly hypointense [78], but components of the tumor may show some uptake of Gd-EOB-DTPA, indicative of a primary liver lesion (Fig. 12).

Summary

Hepatobiliary-specific contrast agents such as Gd-EOB-DTPA have been developed to improve the detection and characterization of focal liver lesions. Because of its distinctive properties, the application of Gd-EOB-DTPA allows comprehensive MRI of the liver and the acquisition of hepatocyte phase images. This provides additional information, especially for the characterization of small focal liver lesions. However, pulse sequence protocols need to be rearranged and contrast injection protocols need to be modified to achieve optimal outcomes. Furthermore, hepatic lesions, both primary and secondary, may appear different on Gd-EOB-DTPA–enhanced MRI starting as early as in the portal venous phase data acquisition. Radiologists must be aware of these differences to detect and characterize focal liver lesions with confidence. The role of Gd-EOB-DTPA in the imaging of other abdominal organs still needs to be evaluated. Also, clinical applications for Gd-EOB-DTPA–enhanced MR cholangiography have not been fully explored; future applications may include the grading of liver function and the diagnosis of sphincter of Oddi dysfunction.

Finally, it is important to note that hepatobiliary phase images need be interpreted in conjunction with all other images. The use of Gd-EOB-DTPA does not change the basic rule that the successful reading of an MR study is based on a multiparametric approach using all the imaging information and not just data acquired during a single series.

References

1. Ba-Ssalamah A, Happel B, Kettenbach J, et al. MRT of the liver: clinical significance of nonspecific and liver-specific MRT contrast agents [in German]. *Radiologe* 2004; 44:1170–1184
2. Semelka RC, Helmberger TK. Contrast agents for MR imaging of the liver. *Radiology* 2001; 218:27–38
3. Shellock FG, Parker JR, Venetianer C, et al. Safety of gadobenate dimeglumine (MultiHance): summary of findings from clinical studies and postmarketing surveillance. *Invest Radiol* 2006; 41:500–509
4. Saito K, Kotake F, Ito N, et al. Gd-EOB-DTPA enhanced MRI for hepatocellular carcinoma: quantitative evaluation of tumor enhancement in hepatobiliary phase. *Magn Reson Med Sci* 2005; 4:1–9
5. Holzapfel K, Breitwieser C, Prinz C, et al. Contrast-enhanced magnetic resonance cholangiography using gadolinium-EOB-DTPA: preliminary experience and clinical applications [in German]. *Radiologe* 2007; 47:536–544
6. Zizka J, Klzo L, Ferda J, et al. Dynamic and delayed contrast enhancement in upper abdominal MRI studies: comparison of gadoxetic acid and gadobutrol. *Eur J Radiol* 2007; 62:186–191
7. van Montfoort JE, Stieger B, Meijer DK, et al. Hepatic uptake of the magnetic resonance imaging contrast agent gadoxetate by the organic anion transporting polypeptide Oatp1. *J Pharmacol Exp Ther* 1999; 290:153–157
8. Takao H, Akai H, Tajima T, et al. MR imaging of the biliary tract with Gd-EOB-DTPA: effect of liver function on signal intensity. *Eur J Radiol* [Epub 2009 Aug 31]
9. Schuhmann-Giampieri G, Mahler M, Rlöl G, Malbauer R, Schmitz S. Pharmacokinetics of the liver-specific contrast agent Gd-EOB-DTPA in relation to contrast-enhanced liver imaging in humans. *J Clin Pharmacol* 1997; 37:587–596
10. Muhler A, Heinzelmann I, Weinmann HJ. Elimination of gadolinium-ethoxybenzyl-DTPA in a rat model of severely impaired liver and kidney excretory function: an experimental study in rats. *Invest Radiol* 1994; 29:213–216
11. Rohrer M, Bauer H, Mintorovitch J, et al. Comparison of magnetic properties of MRI contrast media solutions at different magnetic field strengths. *Invest Radiol* 2005; 40:715–724
12. Schuhmann-Giampieri G, Schmitt-Willich H, Press WR, et al. Preclinical evaluation of Gd-EOB-DTPA as a contrast agent in MR imaging of the hepatobiliary system. *Radiology* 1992; 183:59–64
13. Weinmann HJ, Schuhmann-Giampieri G, Schmitt-Willich H, et al. A new lipophilic gadolinium chelate as a tissue-specific contrast medium for MRI. *Magn Reson Med* 1991; 22:233–237
14. Reimer P, Rummeny EJ, Shamsi K, et al. Phase II clinical evaluation of Gd-EOB-DTPA: dose, safety aspects, and pulse sequence. *Radiology* 1996; 199:177–183
15. Vogl TJ, Kummel S, Hammerstingl R, et al. Liver tumors: comparison of MR imaging with Gd-

EOB-DTPA and Gd-DTPA. *Radiology* 1996; 200:59–67

16. Malone D, Zech CJ, Ayuso C, et al. Magnetic resonance imaging of the liver: consensus statement from the 1st International Primovist User Meeting. *Eur Radiol Suppl* 2008; 18[suppl 4]:849–864
17. Reimer P, Schneider G, Schima W. Hepatobiliary contrast agents for contrast-enhanced MRI of the liver: properties, clinical development and applications. *Eur Radiol* 2004; 14:559–578
18. Frederick MG, McElaney BL, Singer A, et al. Timing of parenchymal enhancement on dual-phase dynamic helical CT of the liver: how long does the hepatic arterial phase predominate? *AJR* 1996; 166:1305–1310
19. Earls JP, Rofsky NM, DeCorato DR, et al. Hepatic arterial-phase dynamic gadolinium-enhanced MR imaging: optimization with a test examination and a power injector. *Radiology* 1997; 202:268–273
20. Zech CJ, Vos B, Nordell A, et al. Vascular enhancement in early dynamic liver MR imaging in an animal model: comparison of two injection regimen and two different doses Gd-EOB-DTPA (gadoxetic acid) with standard Gd-DTPA. *Invest Radiol* 2009; 44:305–310
21. Motosugi U, Ichikawa T, Sou H, et al. Dilution method of gadolinium ethoxybenzyl diethylenetriaminepentaacetic acid (Gd-EOB-DTPA)-enhanced magnetic resonance imaging (MRI). *J Magn Reson Imaging* 2009; 30:849–854
22. Choi JS, Kim MJ, Choi JY, et al. Diffusion-weighted MR imaging of liver on 3.0-Tesla system: effect of intravenous administration of gadoxetic acid disodium. *Eur Radiol* 2010; 20:1052–1060
23. Kim YK, Kwak HS, Kim CS, et al. Detection and characterization of focal hepatic tumors: a comparison of T2-weighted MR images before and after the administration of gadoxectic acid. *J Magn Reson Imaging* 2009; 30:437–443
24. Bollow M, Taupitz M, Hamm B, et al. Gadolinium-ethoxybenzyl-DTPA as a hepatobiliary contrast agent for use in MR cholangiography: results of an in vivo phase-I clinical evaluation. *Eur Radiol* 1997; 7:126–132
25. Lee NK, Kim S, Lee JW, et al. MR appearance of normal and abnormal bile: correlation with imaging and endoscopic finding. *Eur J Radiol* [Epub 2009 Jun 20]
26. Asbach P, Warmuth C, Stemmer A, et al. High spatial resolution T1-weighted MR imaging of liver and biliary tract during uptake phase of a hepatocyte-specific contrast medium. *Invest Radiol* 2008; 43:809–815
27. [No authors listed]. Eovist package insert. Wayne, NJ: Bayer HealthCare Pharmaceuticals, 2008
28. Tschirch FT, Struwe A, Petrowsky H, et al. Contrast-enhanced MR cholangiography with Gd-EOB-DTPA in patients with liver cirrhosis: visualization of the biliary ducts in comparison with patients with normal liver parenchyma. *Eur Radiol* 2008; 18:1577–1586
29. Nikolaou K, Schoenberg SO, Brix, G, et al. Quantification of pulmonary blood flow and volume in healthy volunteers by dynamic contrast-enhanced magnetic resonance imaging using a parallel imaging technique. *Invest Radiol* 2004; 39:537–545
30. Ringe KI, Gupta RT, Brady CM, et al. Respiratory triggered three-dimensional T2-weighted MR cholangiography after the injection of gadoxetate disodium: is it still reliable? *Radiology* 2010; 255:451–459
31. Huppertz A, Balzer T, Blakeborough A, et al. Improved detection of focal liver lesions at MR imaging: multicenter comparison of gadoxetic acid-enhanced MR images with intraoperative findings. *Radiology* 2004; 230:266–275
32. Halavaara J, Breuer J, Ayuso C, et al. Liver tumor characterization: comparison between liver-specific gadoxetic acid disodium-enhanced MRI and biphasic CT—a multicenter trial. *J Comput Assist Tomogr* 2006; 30:345–354
33. Hammerstingl R, Huppertz A, Breuer J, et al. Diagnostic efficacy of gadoxetic acid (Primovist)-enhanced MRI and spiral CT for a therapeutic strategy: comparison with intraoperative and histopathologic findings in focal liver lesions. *Eur Radiol* 2008; 18:457–467
34. El-Serag HB, Mason AC. Rising incidence of hepatocellular carcinoma in the United States. *N Engl J Med* 1999; 340:745–750
35. Lewis KH, Chezmar JL. Hepatic metastases. *Magn Reson Imaging Clin N Am* 1997; 5:319–330
36. Danet IM, Semelka RC, Leonardou P, et al. Spectrum of MRI appearances of untreated metastases of the liver. *AJR* 2003; 181:809–817
37. Stern W, Schick F, Kopp AF, et al. Dynamic MR imaging of liver metastases with Gd-EOB-DTPA. *Acta Radiol* 2000; 41:255–262
38. Zech CJ, Herrmann KA, Reiser MF, et al. MR imaging in patients with suspected liver metastases: value of liver-specific contrast agent Gd-EOB-DTPA. *Magn Reson Med Sci* 2007; 6:43–52
39. Kim YK, Lee JM, Kim CS, et al. Detection of liver metastases: gadobenate dimeglumine-enhanced three-dimensional dynamic phases and one-hour delayed phase MR imaging versus superparamagnetic iron oxide-enhanced MR imaging. *Eur Radiol* 2005; 15:220–228
40. Bartolozzi C, Donati F, Cioni D, et al. Detection of colorectal liver metastases: a prospective multicenter trial comparing unenhanced MRI, MnDPDP-enhanced MRI, and spiral CT. *Eur Radiol* 2004; 14:14–20
41. Takagi H. Diagnosis and management of cavernous hemangioma of the liver. *Semin Surg Oncol* 1985; 1:12–22
42. Gemer O, Moscovici O, Ben-Horin CL, et al. Oral contraceptives and liver hemangioma: a case-control study. *Acta Obstet Gynecol Scand* 2004; 83:1199–1201
43. Sewell JH, Weiss K. Spontaneous rupture of hemangioma of the liver: a review of the literature and presentation of illustrative case. *Arch Surg* 1961; 83:729–733
44. Mergo PJ, Ros PR. Benign lesions of the liver. *Radiol Clin North Am* 1998; 36:319–331
45. Trastek VF, van Heerden JA, Sheedy PF. Cavernous hemangiomas of the liver: resect or observe? *Am J Surg* 1983; 145:49–53
46. Reddy KR, Kligerman S, Levi J, et al. Benign and solid tumors of the liver: relationship to sex, age, size of tumors, and outcome. *Am Surg* 2001; 67:173–178
47. Huppertz A, Haraida S, Kraus A, et al. Enhancement of focal liver lesions at gadoxetic acid-enhanced MR imaging: correlation with histopathologic findings and spiral CT—initial observations. *Radiology* 2005; 234:468–478
48. Brody JM, Schafer L, Tung GA, et al. Conspicuity of liver hemangiomas: short tau inversion recovery, T1, and T2 imaging with gadolinium ethoxybenzyl diethylenetriaminepentaacetic acid. *J Magn Reson Imaging* 2005; 21:391–397
49. Assy N, Nasser G, Djibre A, et al. Characteristics of common solid liver lesions and recommendations for diagnostic workup. *World J Gastroenterol* 2009; 15:3217–3227
50. Lizardi-Cervera J, Cuellar-Gamboa L, Motola-Kuba D. Focal nodular hyperplasia and hepatic adenoma: a review. *Ann Hepatol* 2006; 5:206–211
51. Knowles DM, Wolff M. Focal nodular hyperplasia of the liver: a clinicopathologic study and review of the literature. *Hum Pathol* 1976; 7:533–545
52. Mathieu D, Kobeiter H, Maison P, et al. Oral contraceptive use and focal nodular hyperplasia of the liver. *Gastroenterology* 2000; 118:560–564
53. Nguyen BN, Flejou JF, Terris B, et al. Focal nodular hyperplasia of the liver: a comprehensive pathologic study of 305 lesions and recognition of new histologic forms. *Am J Surg Pathol* 1999; 23:1441–1454
54. Zech CJ, Grazioli L, Breuer J, et al. Diagnostic performance and description of morphological features of focal nodular hyperplasia in Gd-EOB-DTPA-enhanced liver magnetic resonance imaging: results of a multicenter trial. *Invest Radiol* 2008; 43:504–511
55. Marin D, Brancatelli G, Federle MP, et al. Focal nodular hyperplasia: typical and atypical MRI findings with emphasis on the use of contrast media. *Clin Radiol* 2008; 63:577–585
56. Rabe T, Feldmann K, Grunwald K, Runnebaum

B. Liver tumours in women on oral contraceptives. *Lancet* 1994; 344:1568–1569
57. Trotter JF, Everson GT. Benign focal lesions of the liver. *Clin Liver Dis* 2001; 5:17–42
58. Labrune P, Trioche P, Duvaltier I, et al. Hepatocellular adenomas in glycogen storage disease type I and III: a series of 43 patients and review of the literature. *J Pediatr Gastroenterol Nutr* 1997; 24:276–279
59. Grazioli L, Federle MP, Brancatelli G, et al. Hepatic adenomas: imaging and pathologic findings. *RadioGraphics* 2001; 21:877–892
60. Flejou JF, Barge J, Menu Y, et al. Liver adenomatosis: an entity distinct from liver adenoma? *Gastroenterology* 1985; 89:1132–1138
61. Kerlin P, Davis GL, McGill DB, et al. Hepatic adenoma and focal nodular hyperplasia: clinical, pathologic, and radiologic features. *Gastroenterology* 1983; 84:994–1002
62. Colli A, Fraquelli M, Massironi S, et al. Elective surgery for benign liver tumours. *Cochrane Database Syst Rev* 2007; CD005164
63. Deneve JL, Pawlik TM, Cunningham S, et al. Liver cell adenoma: a multicenter analysis of risk factors for rupture and malignancy. *Ann Surg Oncol* 2009; 16:640–648
64. Ringe B, Canelo R, Lorf T, et al. Surgical therapy of benign liver tumors [in German]. *Internist (Berl)* 1997; 38:944–953
65. Choi BY, Nguyen MH. The diagnosis and management of benign hepatic tumors. *J Clin Gastroenterol* 2005; 39:401–412
66. Kim J, Ahmad SA, Lowy AM, et al. An algorithm for the accurate identification of benign liver lesions. *Am J Surg* 2004; 187:274–279
67. Grazioli L, Morana G, Kirchin MA, et al. Accurate differentiation of focal nodular hyperplasia from hepatic adenoma at gadobenate dimeglumine-enhanced MR imaging: prospective study. *Radiology* 2005; 236:166–177
68. Landis SH, Murray T, Bolden S, et al. Cancer statistics, 1998. *CA Cancer J Clin* 1998; 48:6–29
69. Nakeeb A, Pitt HA, Sohn TA, et al. Cholangiocarcinoma: a spectrum of intrahepatic, perihilar, and distal tumors. *Ann Surg* 1996; 224:463–473
70. Olnes MJ, Erlich R. A review and update on cholangiocarcinoma. *Oncology* 2004; 66:167–179
71. Bergquist A, Ekbom A, Olsson R, et al. Hepatic and extrahepatic malignancies in primary sclerosing cholangitis. *J Hepatol* 2002; 36:321–327
72. Bahra M, Langrehr JM, Neuhaus P. Carcinomas of the distal bile duct [in German]. *Chirurg* 2006; 77:335–340
73. Lazaridis KN, Gores GJ. Cholangiocarcinoma. *Gastroenterology* 2005; 128:1655–1667
74. Chung YE, Kim MJ, Park YN, et al. Varying appearances of cholangiocarcinoma: radiologic–pathologic correlation. *RadioGraphics* 2009; 29:683–700
75. Craig JR, Peters RL, Edmondson HA, et al. Fibrolamellar carcinoma of the liver: a tumor of adolescents and young adults with distinctive clinicopathologic features. *Cancer* 1980; 46:372–379
76. McLarney JK, Rucker PT, Bender GN, et al. Fibrolamellar carcinoma of the liver: radiologic–pathologic correlation. *RadioGraphics* 1999; 19:453–471
77. Ba-Ssalamah A, Uffmann M, Saini S, et al. Clinical value of MRI liver-specific contrast agents: a tailored examination for a confident non-invasive diagnosis of focal liver lesions. *Eur Radiol* 2009; 19:342–357
78. Bartolozzi C, Battaglia V, Bozzi E. HCC diagnosis with liver-specific MRI: close to histopathology. *Dig Dis* 2009; 27:125–130

Fig. 1—45-year-old woman with multiple incidentally detected liver lesions at chest CT. Three consecutive axial fat-suppressed T1-weighted 3D gradient-echo data sets were acquired beginning 15 seconds after initiation of gadoxetate disodium. Asterisk marks large cyst in right kidney.
A, Image from early arterial data set shows contrast enhancement predominantly in aorta, which is excellent for vascular assessment but suboptimal for liver lesion detection and characterization.
B, Image from second 3D data set (mid arterial) acquired 23 seconds after contrast initiation shows vivid enhancement of focal nodular hyperplasia (FNH) (*single arrow*) and discrete peripheral enhancement of hemangioma (*double arrow*).
C, Image from third 3D data set (late arterial) acquired 31 seconds after contrast initiation shows continuous enhancement of FNH (*single arrow*) and progressive centripetal enhancement of hemangioma (*double arrow*). Note enhancement of portal venous branches (*arrowheads*).

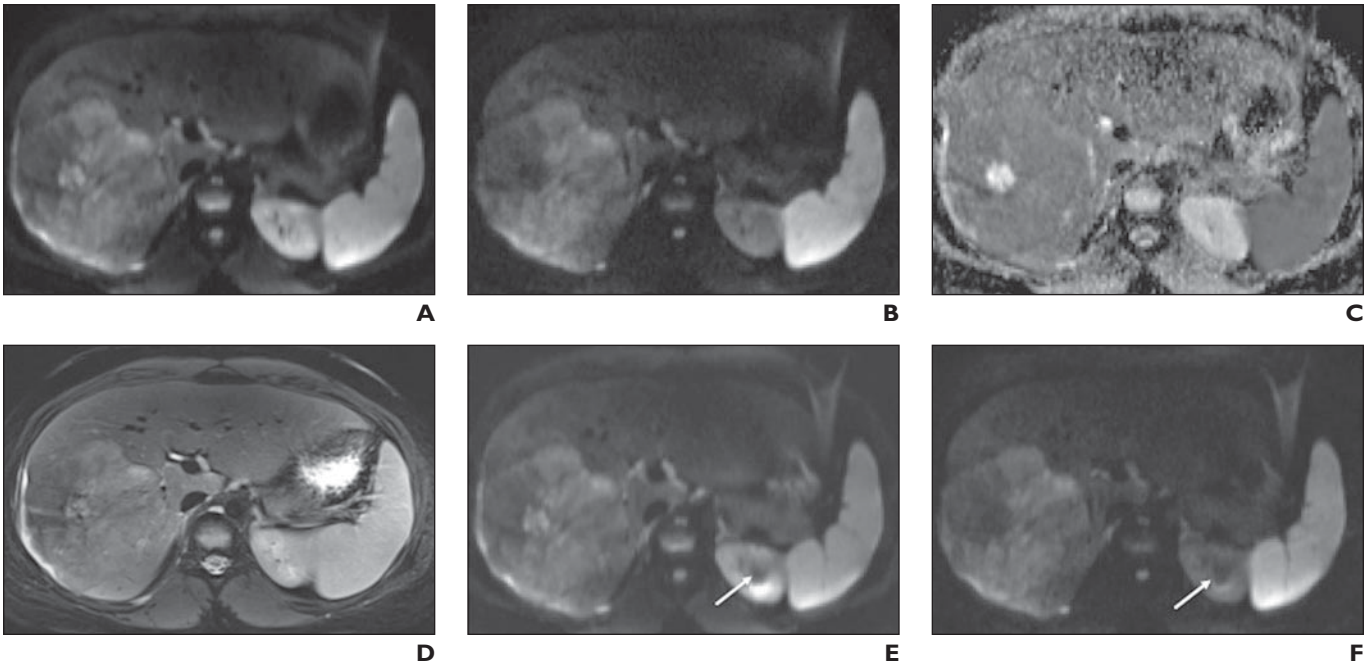

Fig. 2—17-year-old girl with large fibrolamellar carcinoma in right lobe of liver.
A–H, Axial 2D diffusion-weighted images and corresponding apparent diffusion coefficient maps acquired before (**A–C**) and 20 minutes after (**E–G**) initiation of gadoxetate disodium show fibrolamellar carcinoma as heterogeneous mass with restricted diffusion. Note similar appearance of both focal liver lesion and liver itself before and after contrast administration. Note also hypointense appearance of left renal collecting system (*arrow,* **E** and **F**) caused by renal excretion of gadoxetate disodium. Applied b values are 50 s/mm^2 (**A** and **E**) and 800 s/mm^2 (**B** and **F**). In addition, T2-weighted images before (**D**) and after (**H**) contrast injection are shown.

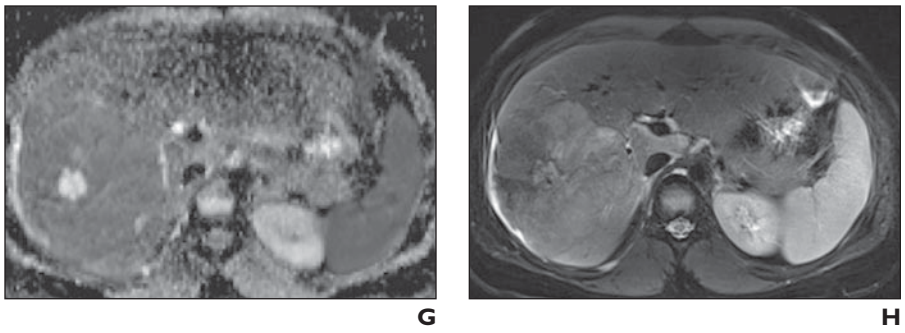

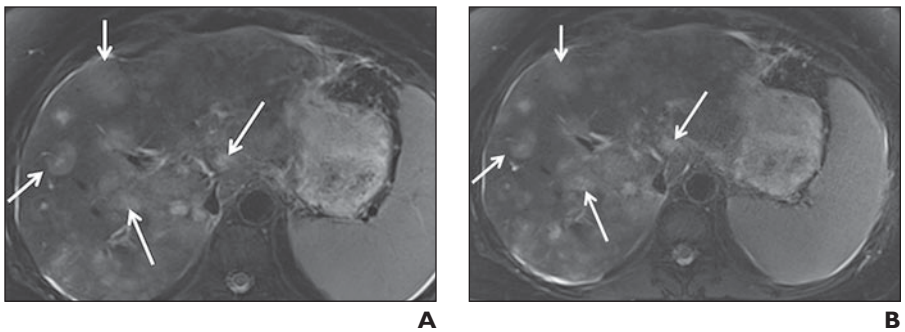

Fig. 3—53-year-old woman with history of colon cancer and multiple liver metastases (*arrows*).
A and **B,** Fat-suppressed axial 2D T2-weighted images acquired before (**A**) and 15 minutes after (**B**) initiation of gadoxetate disodium show no significant difference in lesion conspicuity.

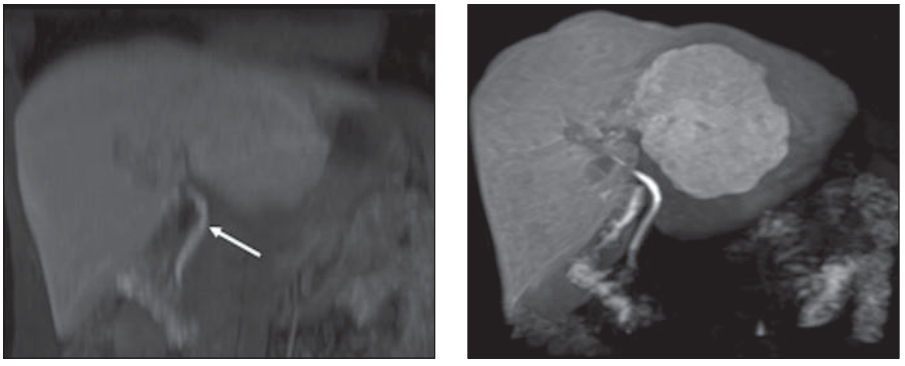

Fig. 4—39-year-old woman with large focal nodular hyperplasia in left hepatic lobe. Coronal maximum intensity projections based on fat-suppressed 3D T1-weighted gradient-echo data sets were acquired 20 minutes after gadoxetate disodium administration.
A and **B,** Source data set image (**A**) was acquired using flip angle of 10°, and source data set image (**B**) was acquired using flip angle of 35°. Use of larger flip angle improves lesion delineation considerably by increasing T1 weighting at expense of reduced background information. Note opacification of common bile duct 20 minutes after contrast injection (*arrow,* **A**).

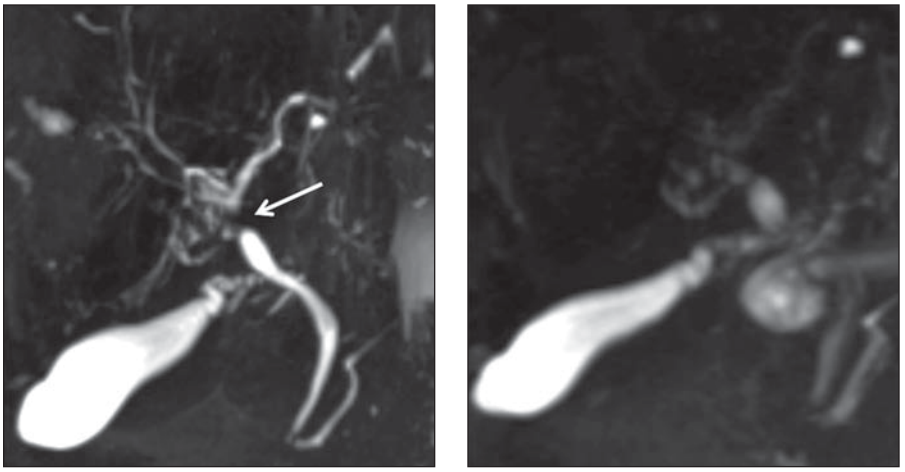

Fig. 5—58-year-old woman with history of breast cancer.
A and **B,** Comparison of coronal T2-weighted 3D MR cholangiography (MRC) images before (**A**) and 10 minutes after (**B**) initiation of gadoxetate disodium. Before contrast injection, entire biliary tract is well visualized. After contrast administration, biliary ductal system cannot be adequately assessed because only segments of common bile duct can be delineated. Note stenosis (*arrow,* **A**) of proximal common hepatic duct, clearly seen on unenhanced MRC image.

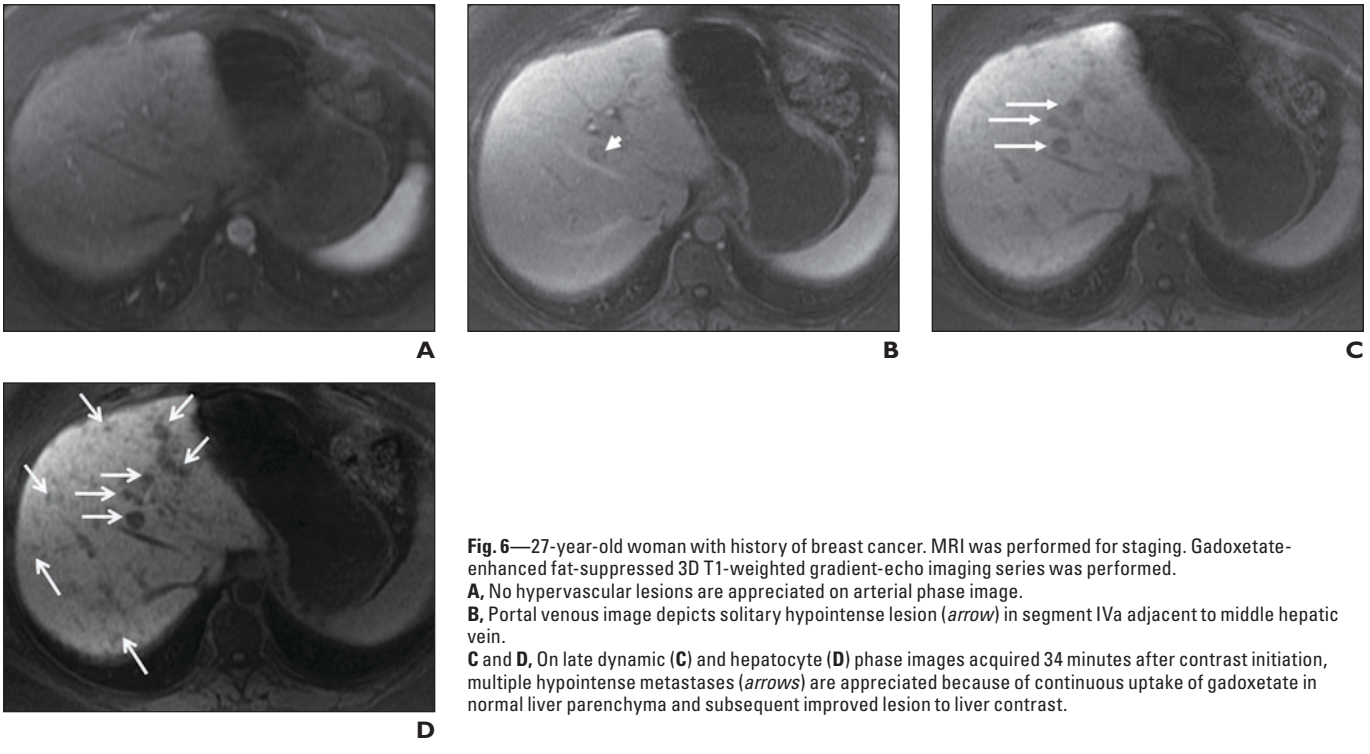

Fig. 6—27-year-old woman with history of breast cancer. MRI was performed for staging. Gadoxetate-enhanced fat-suppressed 3D T1-weighted gradient-echo imaging series was performed.
A, No hypervascular lesions are appreciated on arterial phase image.
B, Portal venous image depicts solitary hypointense lesion (*arrow*) in segment IVa adjacent to middle hepatic vein.
C and **D,** On late dynamic (**C**) and hepatocyte (**D**) phase images acquired 34 minutes after contrast initiation, multiple hypointense metastases (*arrows*) are appreciated because of continuous uptake of gadoxetate in normal liver parenchyma and subsequent improved lesion to liver contrast.

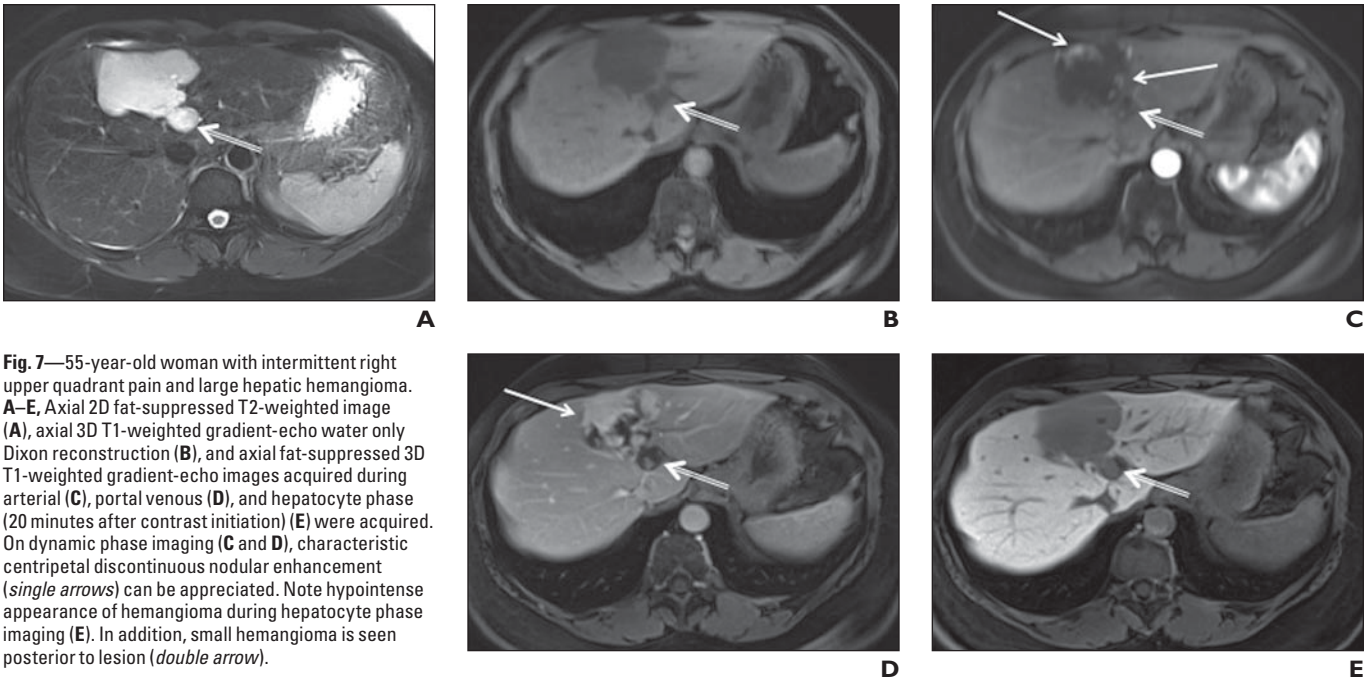

Fig. 7—55-year-old woman with intermittent right upper quadrant pain and large hepatic hemangioma.
A–E, Axial 2D fat-suppressed T2-weighted image (**A**), axial 3D T1-weighted gradient-echo water only Dixon reconstruction (**B**), and axial fat-suppressed 3D T1-weighted gradient-echo images acquired during arterial (**C**), portal venous (**D**), and hepatocyte phase (20 minutes after contrast initiation) (**E**) were acquired. On dynamic phase imaging (**C** and **D**), characteristic centripetal discontinuous nodular enhancement (*single arrows*) can be appreciated. Note hypointense appearance of hemangioma during hepatocyte phase imaging (**E**). In addition, small hemangioma is seen posterior to lesion (*double arrow*).

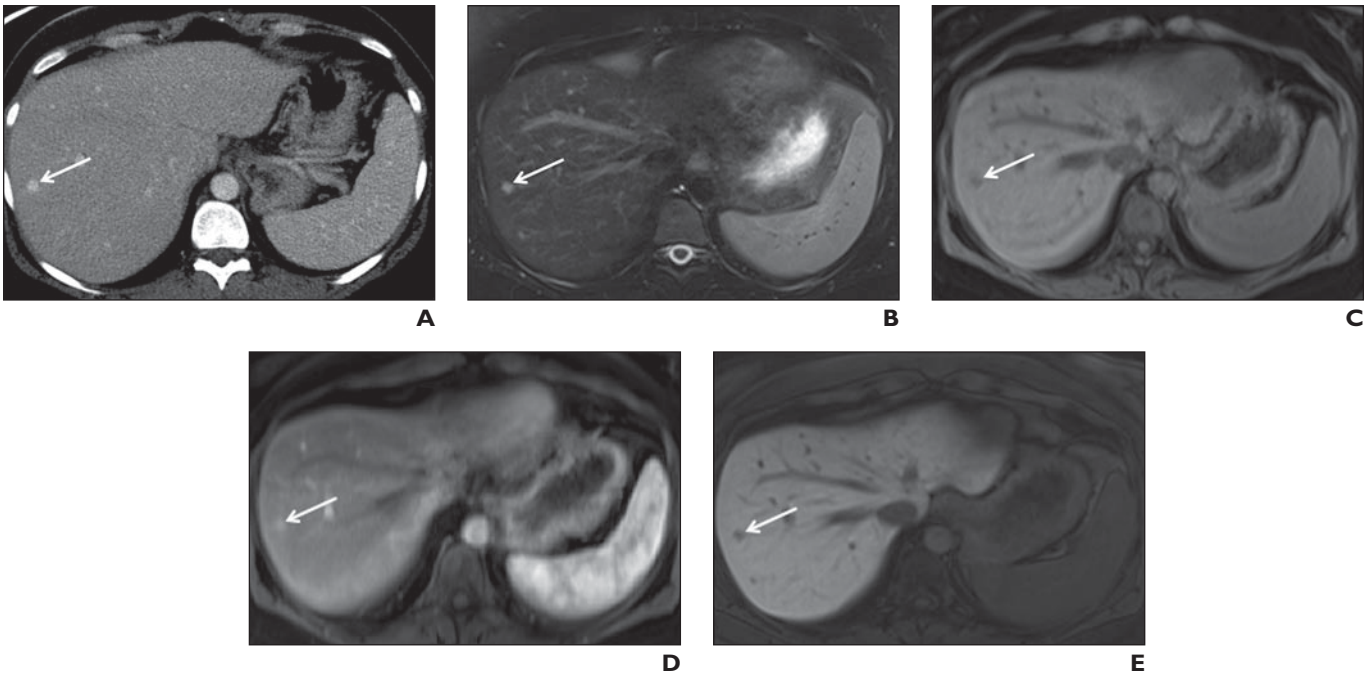

Fig. 8—40-year-old woman with history of malignant spindle cell neoplasm in foot.
A, Axial contrast-enhanced CT image was obtained for staging and depicted solitary hyperintense lesion (*arrow*) in right lobe of liver. Differential diagnoses included hypervascular metastasis and flash-filling hemangioma. MRI with gadoxetate disodium was performed for further characterization of lesion.
B–E, Fat-suppressed axial 2D T2-weighted image (**B**), axial 3D T1-weighted gradient-echo water only Dixon reconstruction (**C**), and axial fat-suppressed 3D T1-weighted gradient-echo images acquired during arterial (**D**) and hepatocyte phase (15 minutes after contrast initiation) (**E**) cannot differentiate between hypervascular metastasis and small flash-filling hemangioma. Arrow indicates solitary hyperdense lesion.

(Fig. 8 continues on next page)

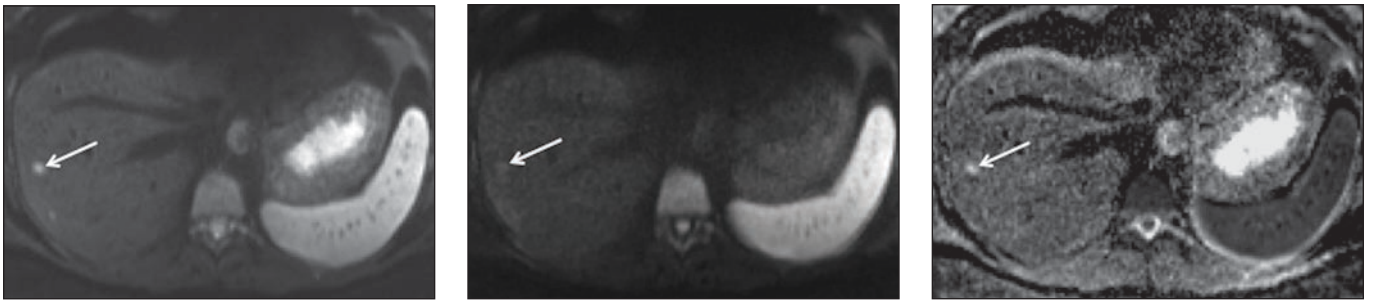

F G H

Fig. 8 (continued)—40-year-old woman with history of malignant spindle cell neoplasm in foot.
F–H, In this scenario, diffusion-weighted imaging (**F** and **G** with b values of 40 and 400 s/mm^2, respectively) proved to be tremendously helpful because corresponding apparent diffusion coefficient map (**H**) shows T2 shine-through, confirming diagnosis of flash-filling hemangioma. Arrow indicates solitary hyperdense lesion.

A B C

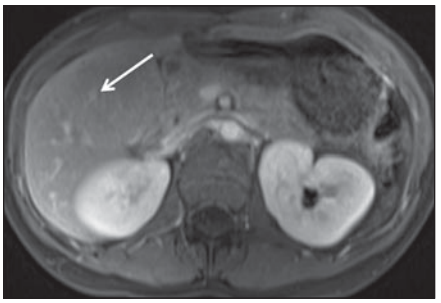

D

Fig. 9—23-year-old woman with focal nodular hyperplasia in left lobe of liver.
A–C, Unenhanced (**A**), late arterial (**B**), and hepatocyte phase (15 minutes after injection of gadoxetate disodium) (**C**) fat-suppressed 3D T1-weighted gradient-echo images show typical vivid enhancement during arterial phase imaging (**B**). On hepatocyte phase imaging, lesion shows fairly characteristic homogeneous popcornlike enhancement. Note central scar (*arrow*), which remains hypointense on hepatocyte phase images.
D, Images **A–C** are in contradiction to classic hyperintense appearance (*arrow*) after injection of extracellular contrast agent (acquired 4 minutes after contrast initiation).

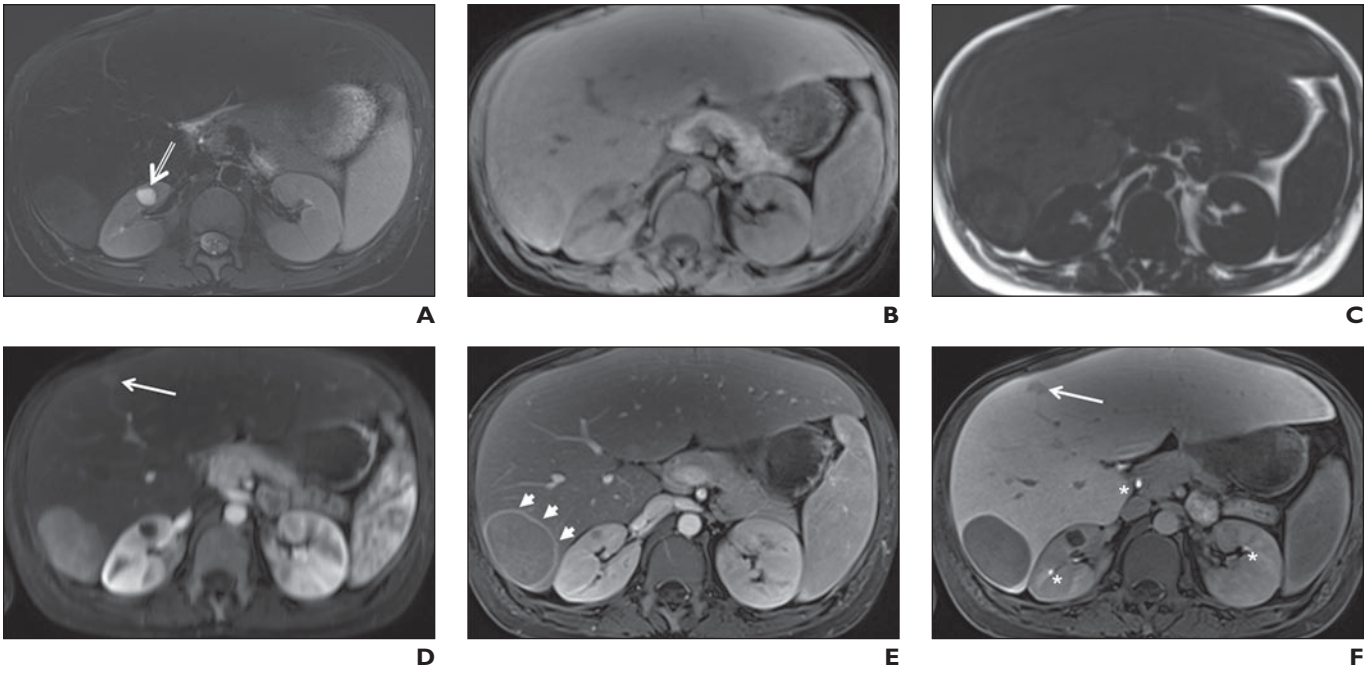

Fig. 10—29-year-old man with glycogen storage disease type 1b and end-stage liver disease.
A–F, Axial fat-suppressed 2D T2-weighted image (**A**), axial 3D T1-weighted gradient-echo water only (**B**) and fat only (**C**) Dixon reconstruction images, and fat-suppressed axial 3D T1-weighted gradient-echo images acquired during arterial phase (**D**), portal venous phase (**E**), and hepatocyte phase (25 minutes after contrast initiation) (**F**) depict hypervascular lesion in posterior right lobe, consistent with hepatic adenoma. Capsule of lesion (*arrows,* **E**) is well appreciated in portal venous phase. Small adenoma with similar image characteristics is seen in segment IVa of liver (*arrow,* **D** and **F**). In addition, small cyst (*arrow,* **A**) can be appreciated in right kidney. Note contrast excretion via biliary system and kidneys on hepatocyte phase image (*asterisks,* **F**). Note also fatty components of lesion on fat only image (**C**) and diffuse fatty infiltration of liver.

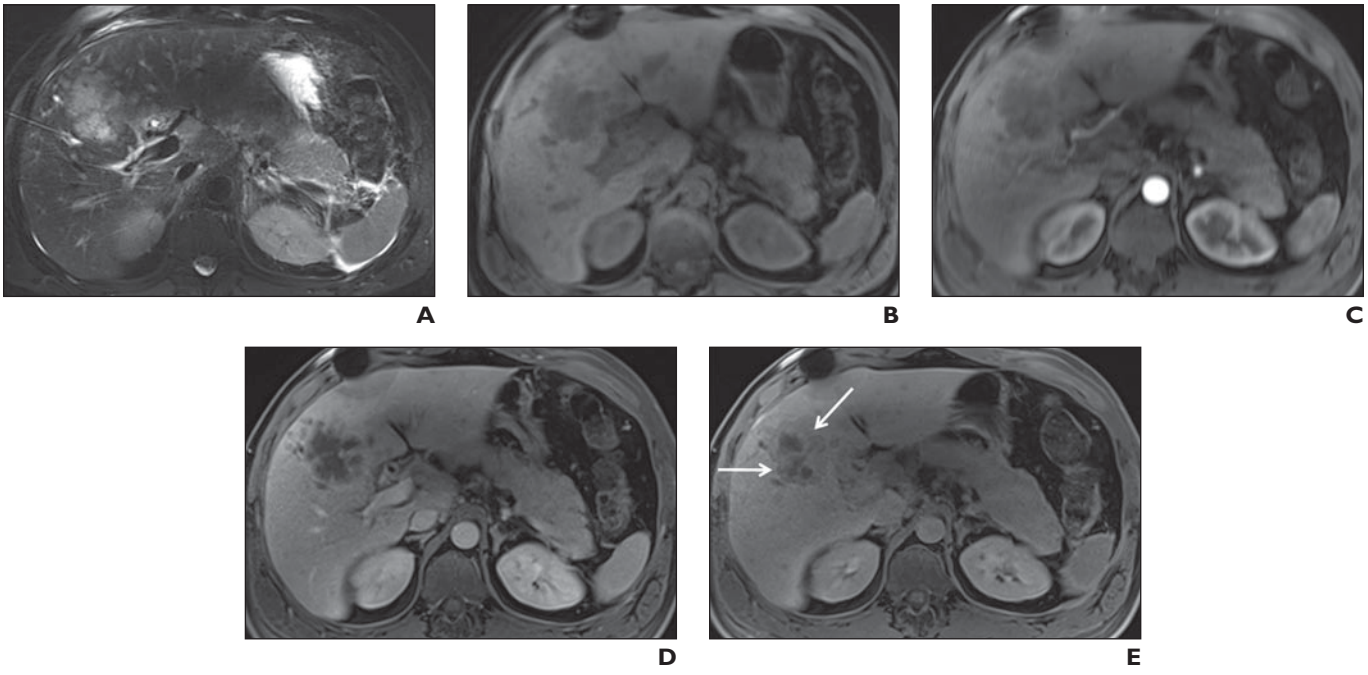

Fig. 11—44-year-old man with peripheral cholangiocarcinoma.
A–E, Fat-suppressed axial 2D T2-weighted image (**A**), axial 3D T1-weighted water only Dixon reconstruction (**B**), and axial fat-suppressed 3D T1-weighted gradient-echo images acquired during early arterial (**C**), portal venous (**D**), and hepatocyte phase (19 minutes after contrast initiation) (**D**) show tumor appears hypointense on unenhanced T1-weighted images and heterogeneously hyperintense on T2-weighted images, respectively. In arterial phase, there is no significant contrast uptake. Note that on hepatocyte phase images, there is some contrast uptake into tumor because of fibrotic components (*arrows,* **E**), but lesion still appears hypointense compared with surrounding liver because of markedly higher uptake of gadoxetate disodium into normal hepatocytes.

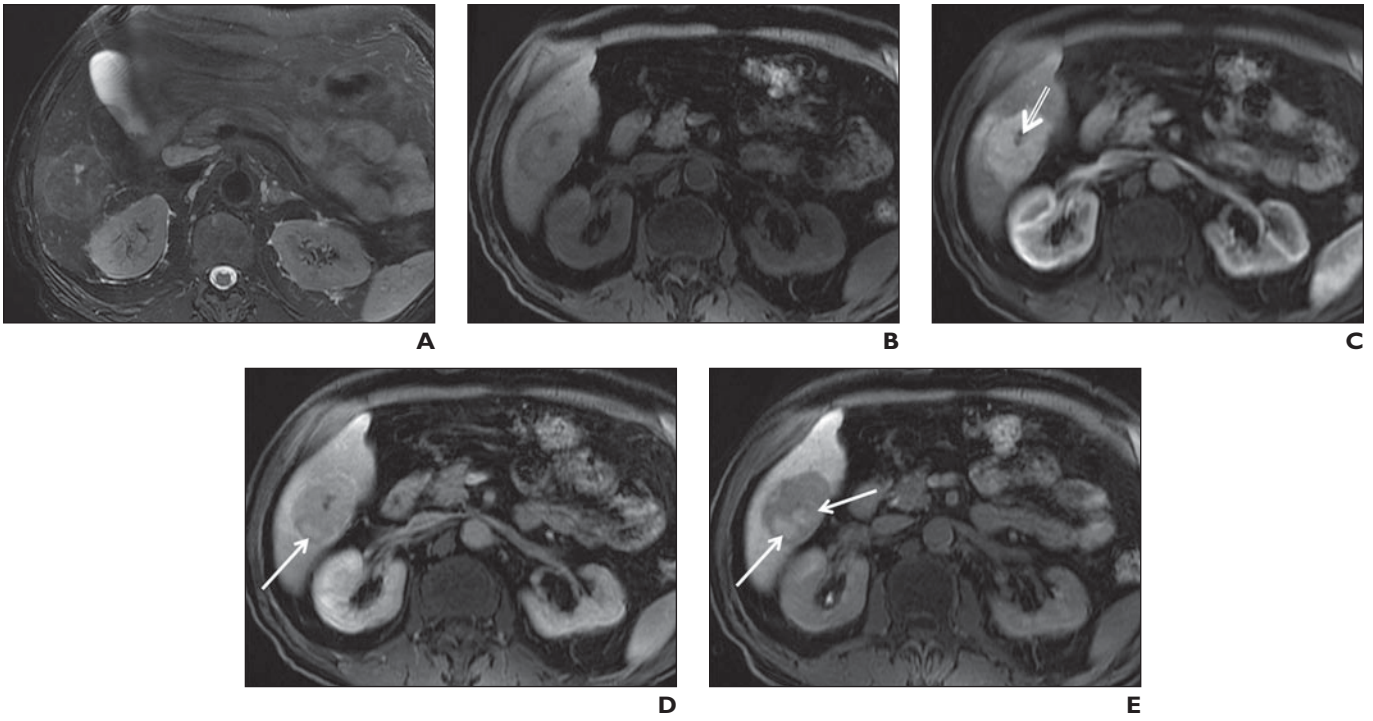

Fig. 12—70-year-old man with fibrolamellar carcinoma in lower right lobe of liver.
A–E, Fat-suppressed axial 2D T2-weighted image (**A**), axial 3D gradient-echo T1-weighted water only Dixon reconstruction (**B**), and axial fat-suppressed 3D T1-weighted gradient-echo images acquired during arterial (**C**), late dynamic (**D**), and hepatocyte phase (15 minutes after contrast initiation) (**E**). In arterial phase, there is distinct uptake of contrast, whereas central scar remains hypointense (*arrow,* **C**). On hepatocyte phase imaging, fibrolamellar carcinoma appears predominantly hypointense to surrounding liver parenchyma. Note focal contrast uptake on late dynamic and hepatocyte phase images (*arrows,* **D** and **E**), which confirms presence of hepatocytes.

FOR YOUR INFORMATION

The reader's attention is directed to part 2 accompanying this article, titled "Gadoxetate Disodium–Enhanced MRI of the Liver: Part 2, Protocol Optimization and Lesion Appearance in the Cirrhotic Liver," which begins on page 29.